

A New Proposal to Jefferson Lab PAC48

Measurement of the Two-Photon Exchange contribution to the electron-neutron elastic scattering cross section

S. Alsalmi (spokesperson)

King Saud University, Riyadh 11451, Saudi Arabia

E. Fuchey (spokesperson) and A.J.R. Puckett*

University of Connecticut, Storrs, Connecticut 06269, USA

B. Wojtsekowski (spokesperson), S. Barcus*, A. Camsonne*, J-P. Chen*,
R. Ent*, D. Gaskell*, O. Hansen*, M. Jones*, C. Keppel*, D. Mack*,
D. Meekins*, R. Michaels*, B. Sawatzky*, G. Smith*, and S. Wood*

Thomas Jefferson National Accelerator Facility, Newport News, Virginia 23606, USA

J. Arrington* and P. Reimer*

Argonne National Laboratory, 9700 S Cass Ave, Lemont, Illinois 60439, USA

T. Averett*

The College of William and Mary, Williamsburg, Virginia 23185, USA

K. Aniol*

California State University, Los Angeles, CA 90032, USA

V. Bellini*

Istituto Nazionale di Fisica Nucleare, I-95123 Catania, Italy

W. Boeglin* and P. Markowitz*

Florida International University, Miami, FL 33199, USA

G. Cates*, K. Gnanvo*, C. Gu*, J. Liu*, N. Liyanage*,
 V. Nelyubin*, D. Nguyen*, and C. Palatchi*

University of Virginia, Charlottesville, Virginia 232904, USA

E. Cisbani*, F. Meddi*, and G. Urciuoli*

Istituto Nazionale di Fisica Nucleare - Sezione di Roma,

P.le Aldo Moro, 2 - 00185 Roma, Italy

J.C. Cornejo* and B. Quinn*

Carnegie Mellon University, Pittsburgh, Pennsylvania 15213, USA

B. Crowe* and B. Vlahovic*

North Carolina Central University, Durham, North Carolina 27707, USA

D. Hamilton* and R. Montgomery*

*SUPA School of Physics and Astronomy,
 University of Glasgow, Glasgow G12 8QQ, UK*

F. Hauenstein*

Old Dominion University, Norfolk, Virginia 23529, USA

C. Petta* and C. Suttera*

Istituto Nazionale di Fisica Nucleare, Dipt. di Fisica dell Univ. di Catania, I-95123 Catania, Italy

G.G. Petratos*

Kent State University, Kent, OH 44242, USA

A. Sarty*

Saint Mary's University, Halifax, Nova Scotia B3H 3C3, Canada

K. Slifer*

University of New Hampshire, Durham, NH 03824, USA

A. Shahinyan*

AANL, 2 Alikhanian Brothers Street, 0036, Yerevan, Armenia

S. Širca*

Faculty of Mathematics and Physics, University of Ljubljana, 1000 Ljubljana, Slovenia

E. Voutier*

Institut de Physique Nucléaire, 15 Rue Georges Clemenceau, 91400 Orsay, France

(Dated: June 10, 2020)

Abstract

We propose make a high precision measurement of the two-photon exchange contribution (TPE) in elastic electron-neutron scattering at a four-momentum transfer $Q^2 = 4.5$ $(\text{GeV}/c)^2$. While significant efforts to study the two-photon-exchange have focused around elastic electron-proton scattering, the impact of TPE on neutron form factors was never examined experimentally. The proposed experiment will provide the very first assessment of the two-photon exchange in electron-neutron scattering, which will be important for understanding of the nucleon form factor physics.

The proposed experiment will be performed in Hall A using the BigBite (BB) spectrometer to detect the scattered electrons and the Super-BigBite (SBS) to detect the protons and neutrons. The experiment should run concurrently with the E12-09-019 G_M^n and E12-17-004 G_E^n -Recoil experiments, which are expected to run in 2021. The experimental setup of the proposed experiment will be identical to that of E12-09-019 experiment.

The “ratio” method will be used to extract the electric form factor of the neutron G_E^n by scattering unpolarized electrons from deuterium quasi-elastically at two beam energies 4.4 and 6.6 GeV and electron scattering angles 41.9 and 23.3 degrees respectively. In the proposed approach, systematic errors are greatly reduced compared to those in the traditional single electron arm configuration. Several experiments at Mainz and JLab have used the ratio method to measure the neutron magnetic form factor in the past years. The method can be extended to extract the neutron electric form factor even with less stringent requirements on the knowledge of the absolute neutron detection efficiency and experimental kinematics.

I. INTRODUCTION

In 1950's, a series of experiments performed by R. Hofstadter [1] revealed that the nucleons have a substructure (would be called later the quarks and gluons). The experiment confirmed M. Rosenbluth's theory [2] based on one-photon exchange approximation. In the Born approximation, where the interaction between the electron and the nucleon occurs *via* an exchange of a one virtual photon (OPE), the unpolarized $e - N$ elastic cross section can be expressed in terms of a nucleon magnetic, G_M , and electric, G_E , form factors. These form factors describe the deviation from a point-like scattering cross section:

$$\left(\frac{d\sigma}{d\Omega} \right)_{eN \rightarrow eN} = \frac{\sigma_{Mott}}{\epsilon(1 + \tau)} [\tau \cdot G_M^2(Q^2) + \epsilon \cdot G_E^2(Q^2)] = \sigma_T + \epsilon \cdot \sigma_L, \quad (1)$$

where E and E' are the incident and scattered electron energies, respectively, θ is the electron scattering angle, $\tau \equiv -q^2/4M^2$, with $-q^2 \equiv Q^2 = 4EE' \sin(\theta/2)$ being the negative four momentum transfer square, M is the nucleon mass, and $\epsilon = [1 + 2(1 + \tau) \tan^2(\theta/2)]^{-1}$ is the longitudinal polarization of the virtual photon, σ_L and σ_T are the cross sections for longitudinally and transversely polarized virtual photons, respectively.

14

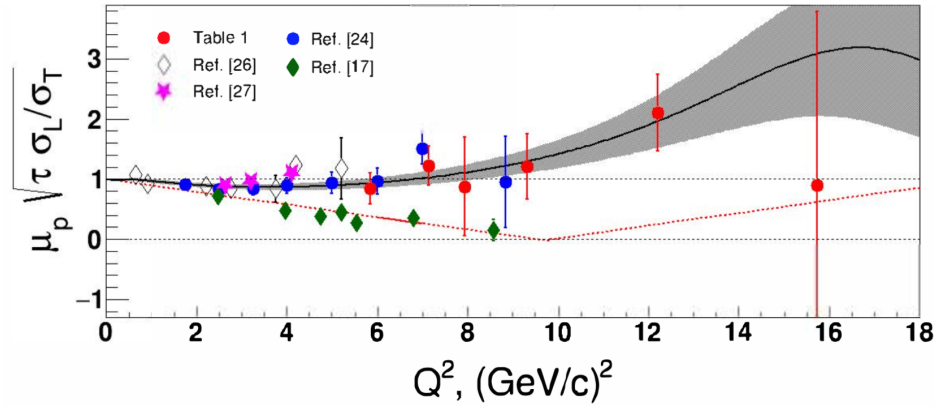


FIG. 1. The square root of Rosenbluth slope, corrected for kinematical factor $\sqrt{\tau}$ and μ_p , observed in elastic electron-proton scattering, adopted from Ref. [3].

The linear ϵ dependence of the cross section is due to σ_L term, see Eq. 1. The ratio σ_L/σ_T

is a Rosenbluth slope related to G_E/G_M (in OPE), see Fig. 1. The data show that at Q^2 of 4-5 $(\text{GeV}/c)^2$ the Rosenbluth slope is three-four times larger than it suppose to be (in OPE) for the observed values of the G_E^p/G_M^p ratio.

The nucleon electromagnetic form factors can reveal a lot of information about the nucleon internal structure, as well as the quark distribution. The form factors depend only on one variable the negative square of the four-momentum transfer carried by the photon, Q^2 . In the limit of large Q^2 , pQCD provides well-motivated predictions for the Q^2 -dependance of the form factors and their ratio. However, it was never predicted at what Q^2 range the pQCD prediction (scaling) will be valid. Studies of GPDs show that pQCD validity will require a very large Q^2 of 100 $(\text{GeV}/c)^2$. It was discovered at JLab, using the double polarization methods, that the proton electric and magnetic form factors behave differently starting at $Q^2 \approx 1 (\text{GeV}/c)^2$.

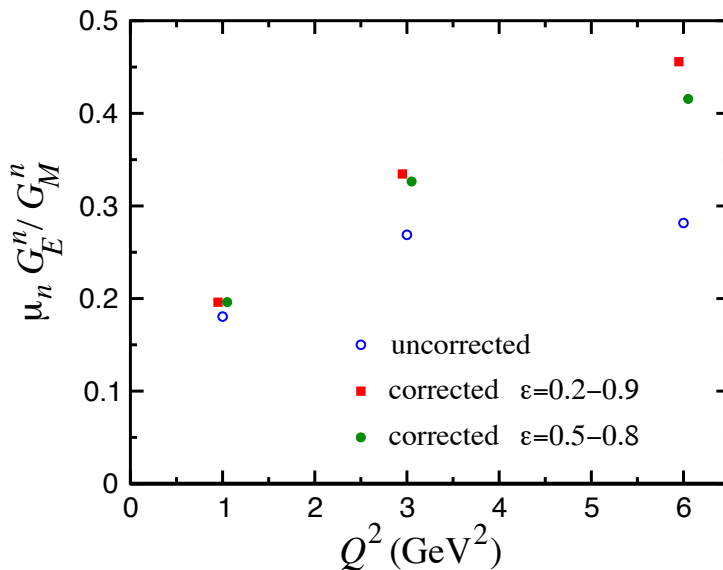


FIG. 2. Projected impact of TPE on G_E^n/G_M^n using LT separation, according to Ref. [4].

Experimentally, the nucleon form factors can be measured using one of two techniques: polarization transfer technique and Rosenbluth technique. The polarization method examines the polarization transfer from longitudinally polarized electron to the recoiling nucleon

and determine the resulting azimuthal asymmetry distribution using a polarimeter. Alternatively, one can use the polarized electron beam and a polarized target. While in the Rosenbluth method, the electric and magnetic form factors can be separated by making two or more measurements with different ϵ values (*i.e.* different beam energies and angles), but with same Q^2 value. Rosenbluth technique requires an accurate measurement of the cross section and suffers from large systematic uncertainties arising from several factors. For instance, an accurate knowledge of the neutron detector efficiency is required.

When comparing the values of G_E^p/G_M^p obtained from both techniques, a significant discrepancy was observed (see Fig. 1). Such discrepancy implies a potential problem in our understanding of the nucleon substructure. Many efforts were made in order to provide legitimate explanation, and it is believed that the inconsistency is due to contribution of two-photon exchange in $e - N$ elastic scattering process, see Refs. [5, 6]. Predictions made for the neutron case are shown in Fig. 2, adopted from [4]. The contribution of TPE could reach about 30% of Rosenbluth slope value at 5 (GeV/c)².

In the following we propose to make precision L/T separation of the elastic electron-neutron cross section and first experimental assessment of the two-photon exchange contribution on the neutron magnetic form factor measurements (see also Ref. [7]). The result of the nTPE experiment will likely add a new component to our understanding of the elastic electron-nucleon process.

50

II. PHYSICS MOTIVATION

51 The nucleon plays the same central role in hadronic physics that the hydrogen atom does
 52 in atomic physics and the deuteron in the physics of nuclei. The structure of the nucleon
 53 and its general properties, such as (static) charge, magnetic moment, size, mass, and the
 54 form factors and structure functions, are of fundamental scientific interest. The nucleon is a
 55 laboratory for the study of the quark-gluon interaction and both nucleons, the proton and
 56 the neutron, need to be explored. At present the proton has been more thoroughly studied
 57 at large Q^2 than the neutron. More data on the neutron is essential if we are to make real
 58 progress in obtaining a complete description of the quark structure of the nucleon [8].

59 Considerable information on the structure of the nucleon has been obtained by using
 60 electromagnetic probes via electron scattering. Inclusive deep inelastic scattering (DIS) has
 61 been a classical tool with which the partonic structure of the nucleon has been probed. At
 62 high Q^2 , DIS yields information on the light-cone momentum space distributions of quarks
 63 and gluons in the nucleon when viewed through the infinite momentum frame. Many of the
 64 experimental foundations of QCD are in fact derived from investigations of various aspects
 65 of DIS.

66 Exclusive processes, on the other hand, such as elastic electron and photon scattering,
 67 can provide information on the spatial distribution of the nucleon's constituents, which is
 68 parameterized through the elastic nucleon form factors. Experimental studies of elastic
 69 electron scattering from both the proton and the neutron were initiated at SLAC and are
 70 now being thoroughly performed at Jefferson Lab and other facilities world-wide.

71 The Dirac form factor, F_1 , describes the distribution of the electric charge, while the
 72 helicity non-conserving Pauli form factor, F_2 , describes the distribution of the magnetic
 73 moment; these two form factors are the ingredients of the hadronic current. These currents
 74 contain information on the transverse charge distribution for an unpolarized and transversely
 75 polarized nucleon, respectively, in the infinite momentum frame [9, 10].

76 The Sachs form factors, G_E and G_M , the ratio of which will be extracted directly from

⁷⁷ our data for the neutron, are related to F_1 and F_2 by

$$F_1 = \frac{G_E + \tau G_M}{1 + \tau} \text{ and } F_2 = \frac{G_M - G_E}{\kappa(1 + \tau)}, \quad (2)$$

⁷⁸ where κ is the nucleon anomalous magnetic moment.

⁷⁹ At asymptotically high Q^2 , one can apply perturbative QCD (pQCD) to describe the
⁸⁰ Q^2 dependence of exclusive electron scattering. Early attempts to determine the scaling
⁸¹ behavior for F_1 were performed by using a simple dimensional counting rule justified by the
⁸² inclusion of two gluon exchange processes [? ?].

⁸³ A recent calculation by Belitski *et al.* [?] was performed where quark orbital angular
⁸⁴ momentum was included to determine the behavior for the non-helicity conserving form
⁸⁵ factor F_2 . It was found to logarithmic accuracy that the ratio F_2/F_1 should, at high Q^2 ,
⁸⁶ follow the form

$$\frac{F_2}{F_1} \propto \frac{\log^2(Q^2/\Lambda^2)}{Q^2}, \quad (3)$$

⁸⁷ This behavior was found to set in surprisingly early for the proton data for $Q^2 > 2.0 \text{ GeV}^2$
⁸⁸ with $\Lambda \approx 300 \text{ MeV}$. Using preliminary G_E^n data from E02-013 up to 3.5 GeV^2 , this scaling
⁸⁹ had not yet been observed [?] suggesting pQCD has not yet set in at this range in Q^2 .
⁹⁰ A calculation from ANL utilizing a Poincare invariant truncated Faddeev equation for a
⁹¹ quark-diquark system [?] suggests this type of behavior for each of the two nucleons may
⁹² be expected. For high Q^2 , this experiment in conjunction with high $Q^2 G_M^n$ data may be
⁹³ able to observe the onset of this pQCD behavior in the neutron form factors.

⁹⁴ Over the years many QCD-inspired models have been developed to describe nucleon
⁹⁵ electromagnetic form factors at small and intermediate Q^2 values ($Q^2 < 1-2 \text{ GeV}^2$). While
⁹⁶ these have provided some insights into the possible origin of the nonperturbative quark
⁹⁷ structure of the nucleon, ultimately one would like to use experimental form factor data to
⁹⁸ test the workings of QCD itself.

⁹⁹ Recently, important developments in QCD phenomenology has been the exploration of
¹⁰⁰ the generalized parton distribution (GPD) formalism [? ? ?], which provides relations
¹⁰¹ between inclusive and exclusive observables. The nucleon elastic form factors F_1 and F_2 are

¹⁰² given by the first moments of the GPDs

$$F_1(t) = \sum_q \int_0^1 H^q(x, \xi, t, \mu) dx \quad \text{and} \quad F_2(t) = \sum_q \int_0^1 E^q(x, \xi, t, \mu) dx, \quad (4)$$

¹⁰³ where H^q and E^q are two of the generalized parton distributions, x is the standard Bjorken
¹⁰⁴ x , ξ is the “skewness” of the reaction (Fig. ??), t is the four-momentum transferred
¹⁰⁵ by the electron, μ is a scale parameter necessary from the evolution over Q^2 , analogous to
¹⁰⁶ DIS parton distributions, and the sum is over all quarks and anti-quarks. These may be
¹⁰⁷ accessed through processes such as deeply virtual compton scattering, where the interaction
¹⁰⁸ is factorized into a hard part with the virtual photon/photon interactions with an individual
¹⁰⁹ quark and a soft part of the residual system where the GPD information is contained, Fig. ??.

¹¹⁰ Furthermore, as shown earlier by Ji [?], the moments of GPDs can yield information,
¹¹¹ according to the Angular Momentum Sum Rule, on the contribution to the nucleon spin
¹¹² from quarks and gluons, including both the quark spin and orbital angular momentum.

¹¹³ At present, experimental measurements of GPDs are scarce. Until such data becomes
¹¹⁴ available, work has been done to attempt to parameterize these GPDs, which rely heavily on
¹¹⁵ data from electromagnetic form factors and parton distributions from DIS as constraints [? ¹¹⁶ ? ?]. Data at high Q^2 for G_E^n would contribute significantly in the development of these
¹¹⁷ models.

¹¹⁸ The isovector and isoscalar form factors constructed from the proton and neutron form
¹¹⁹ factors have different sensitivity to higher Fock components of the light cone quark wave
¹²⁰ function. This difference can be an important handle to test the valence quark dominance in
¹²¹ exclusive reactions in the few $(\text{GeV}/c)^2$ range. Data on F_{1p} and F_{1n} will allow the extraction
¹²² of information related to the $(u-d)$ distribution, which was calculated recently using the GPD
¹²³ approach by K. Goeke, M. Polyakov, and M. Vanderhaeghen [?].

¹²⁴ Recent theoretical developments also indicate that measurements of the individual elastic
¹²⁵ form factors of the nucleon up to high Q^2 may shed light on the problem of nucleon spin [? ¹²⁶].

¹²⁷ As an incidental benefit of the proposed experiment, a better determination of the neutron
¹²⁸ electric form factor will be very important for calculations of nuclear form factors, such as

₁₂₉ those of the deuteron. Even though $G_E^n \ll G_E^p$ at $Q^2 \approx 0$, at larger Q^2 ($Q^2 \sim 3 \text{ GeV}^2$) the ratio
₁₃₀ G_E^n/G_E^p can be as large as ≈ 0.4 , so that accurate information on G_E^n at large Q^2 is essential
₁₃₁ for a reliable description of the deuteron form factors.

132

III. TECHNIQUE

133 The neutron form factors are challenging to be determine experimentally especially be-
 134 cause there is no free neutron target. However, since the deuterium is a loosely coupled
 135 system, it can be viewed as the sum of a proton target and a neutron target. In fact, quasi-
 136 elastic scattering from deuterium has been used to extract the neutron magnetic form factor,
 137 G_M^n , at modestly high Q^2 for decades [11, 12] in the single arm (e, e') experiments. How-
 138 ever, the proton cross section needs to be subtracted by applying a single-arm quasi-elastic
 139 electron-proton scattering. This “proton-subtraction” technique suffers from a number sys-
 140 tematic uncertainties e.g. contributions from inelastic and secondary scattering processes.

141 Many year ago, L. Durand [13] proposed the so-called “ratio-method” based on the mea-
 142 surement of both $D(e, e'n)$ and $D(e, e'p)$ reactions. In this method, many of the systematic
 143 errors are cancel out. Several experiments [14–16] have applied the ratio-method to determine
 144 the neutron magnetic form factor. We propose to use this method to measure Rosenbluth
 145 slope and extract (in OPE approximation) the neutron electric form factor, G_E^n .

146 Data will be collected for quasi-elastic electron scattering from deuteron in process
 147 $D(e, e'n)p$. A complementary $D(e, e'p)n$ data will be taken to calibrate the experiment ap-
 148 paratus. The current knowledge of the $e - p$ elastic scattering cross section (obtained in the
 149 single arm $H(e, e')p$ and $H(e, p)e'$ experiments) will be also used for precision determination
 150 the experiment kinematics.

151 Applying Rosenbluth technique to measure G_E^n requires accurate measurement of the cross
 152 section and suffers from large uncertainties. To overcome this issue, we propose to extract
 153 the value of G_E^n from the measured the ratio of quasi-elastic yields, $R_{n/p}$, in scattering from
 154 a deuteron target as follows:

$$R_{n/p} \equiv R_{observed} = \frac{N_{e, e'n}}{N_{e, e'p}} \quad (5)$$

155 $R_{observed}$ needs to be corrected to extract the ratio of e-n/e-p scattering from nucleons:

$$R_{corrected} = f_{corr} \times R_{observed} , \quad (6)$$

156 where the correction factor $f_{correction}$ takes into account the variation in the hadron efficiencies
 157 due to changes of $e - N$ Jacobian, the radiative corrections, and absorption in path from the
 158 target to the detector, and small re-scattering correction.

159 In one-photon approximation, $R_{corrected}$ can be presented as:

$$R_{corrected} = \frac{\sigma_{Mott}^n \cdot (1 + \tau_p)}{\sigma_{Mott}^p \cdot (1 + \tau_n)} \times \frac{\epsilon \sigma_L^n + \sigma_T^n}{\epsilon \sigma_L^p + \sigma_T^p} \quad (7)$$

It is important that the ratio $R_{Mott} = \frac{\sigma_{Mott}^n \cdot (1 + \tau_p)}{\sigma_{Mott}^p \cdot (1 + \tau_n)}$ could be determined with very high relative accuracy even with modest precision for the beam energy, electron scattering angle, and detector solid angle. Now, let us write the $R_{corrected}$ at two values of ϵ using $R_c^{n(p)} = \sigma_L^{n(p)} / \sigma_T^{n(p)}$ as:

$$R_{corrected,\epsilon_1} = R_{Mott,\epsilon_1} \times \frac{\epsilon_1 \sigma_L^n + \sigma_T^n}{\epsilon_1 \sigma_L^p + \sigma_T^p} \quad R_{corrected,\epsilon_2} = R_{Mott,\epsilon_2} \times \frac{\epsilon_2 \sigma_L^n + \sigma_T^n}{\epsilon_2 \sigma_L^p + \sigma_T^p}$$

In these two equations there are two unknown variables: σ_L^n and σ_T^n . The dominant contribution to the uncertainty of the slope of the cross section vs. ϵ , $S_c^n = \sigma_L^n / \sigma_T^n$, will come from the uncertainty of S_c^p . At $Q^2=4.5$ (GeV/c)², according to the global analysis of $e - p$ cross section [3], the value of S_c^p is close to $1/(\tau \mu_p^2) = 0.107$ with uncertainty of 0.01. The resulting equation for S_c^n is:

$$A = B \times \frac{1 + \epsilon_1 S_c^n}{1 + \epsilon_2 S_c^n} \approx B \times (1 + \Delta \epsilon \cdot S_c^n),$$

160 where the variable $A = R_{corrected,\epsilon_1} / R_{corrected,\epsilon_2}$ will be measured with relative precision of
 161 0.1%. Assuming, for this estimate, equal values of Q^2 for two kinematics, the τ and σ_T for
 162 two kinematics are canceled out, and the variable $B = R_{Mott,\epsilon_1} / R_{Mott,\epsilon_2} \times (1 + \epsilon_2 S_c^p) / (1 + \epsilon_1 S_c^p)$.
 163 For actual small range of ϵ and small value of the slope, the $B \approx (1 - \Delta \epsilon \cdot S_c^p)$. The value
 164 of B will be determined from global proton $e - p$ data to a precision of 0.25×0.01 .

165 At $Q^2=4.5$ (GeV/c)² the ratio $\mu_n G_E^n / G_M^n$ is of 0.55 ± 0.05 , see the review [17]. In a
 166 simplest model, the slope S_c^n is a sum of the slope due to G_E^n / G_M^n and the TPE contribution.
 167 If we use for TPE the prediction [4], shown in Fig. 2, the TPE leads to increase of S_c^n by a
 168 factor of 2, so the result of this experiment for TPE will be $0.069 \pm 0.012 \pm 0.01$, where the
 169 first uncertainty is due to accuracy of G_E^n / G_M^n and the second one due to projected precision
 170 of this experiment. It would be a 4-4.5 sigma observation of the neutron TPE.

171

IV. EXPERIMENTAL SETUP

172 As illustrated in Fig. 3, this experiment will study electron scattering from a 15 cm
 173 long liquid Deuterium target held in a vacuum. The scattered electron will be detected
 174 in the BigBite spectrometer with an upgraded electron detector stack. The neutron arm is
 175 arranged with a dipole magnet 48D48 (SBS) and a segmented hadron calorimeter HCAL. The
 176 whole detector package was designed and is now under assembling for the GMn, E12-09-019,
 177 experiment.

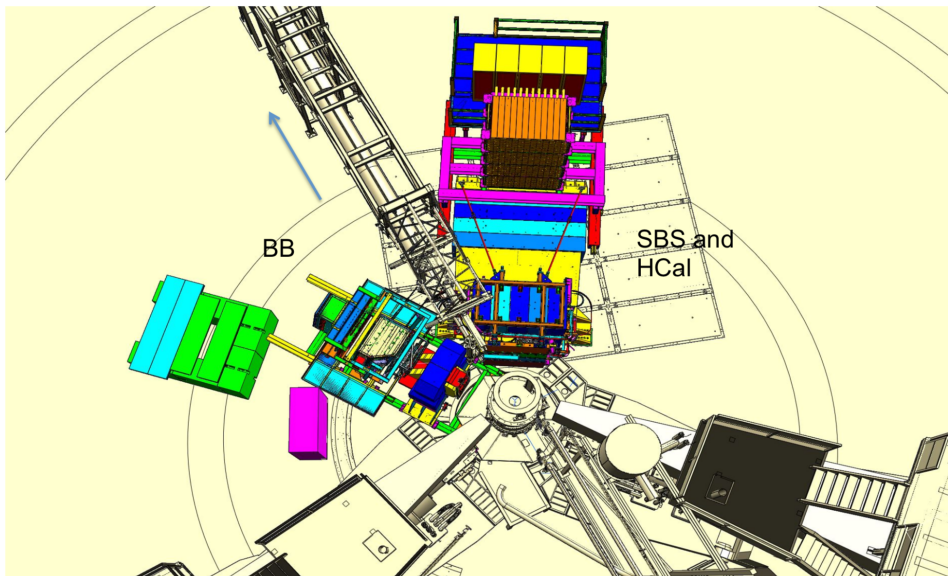


FIG. 3. Layout of the experimental setup in nTPE.

178

1. Parameters of the SBS

179 The 48D48 magnet from Brookhaven was acquired as part of the Super Bigbite project
 180 and will be available for this experiment. It consists of a large dipole magnet which provides
 181 a field integral of about $1.7 \text{ T} \cdot \text{m}$, allowing for quasielastic protons to be sufficiently deflected
 182 to allow clear differentiation from neutrons. The active field volume has an opening of $46 \times$
 183 $25 \text{ vertical} \times \text{horizontal}$), matching the aspect ratio of the neutron arm, and a depth of 48
 184 cm.

185 The placement of this magnet will be 1.6 m away from the target, which would normally
186 interfere with the beamline. To accommodate this, modifications were made to the iron yoke
187 such that the beamline will pass through the magnet yoke area.

188 The field configuration will be such that positively charged particles will be deflected
189 upwards away from the hall floor. For a field integral of 1.7 Tesla-m, protons of momentum
190 2.5 GeV/c will be deflected 250 mrad, which translates to a displacement of xxm. Including
191 expected detector resolution, the $p_{miss,\perp}$ distribution will be similar to what was seen in
192 E02-013, so cuts of < 100 MeV/c will be appropriate. Monte Carlo simulations show a
193 contamination of charged quasielastics to be negligible.

194 The presence of the magnet also works to sweep low energy charged particles from the
195 target away from the neutron arm. Particles of momentum less than 1.3 GeV/c will be
196 entirely swept outside of the neutron arm acceptance. This greatly reduces the amount of
197 charged low energy background.

198

A. The BigBite Spectrometer

199 Scattered electrons will be detected in the BigBite spectrometer. The spectrometer con-
 200 sists of a single dipole magnet (with magnetic field approximately 1.2 Tesla-m and a detection
 201 system, see Fig. 4.

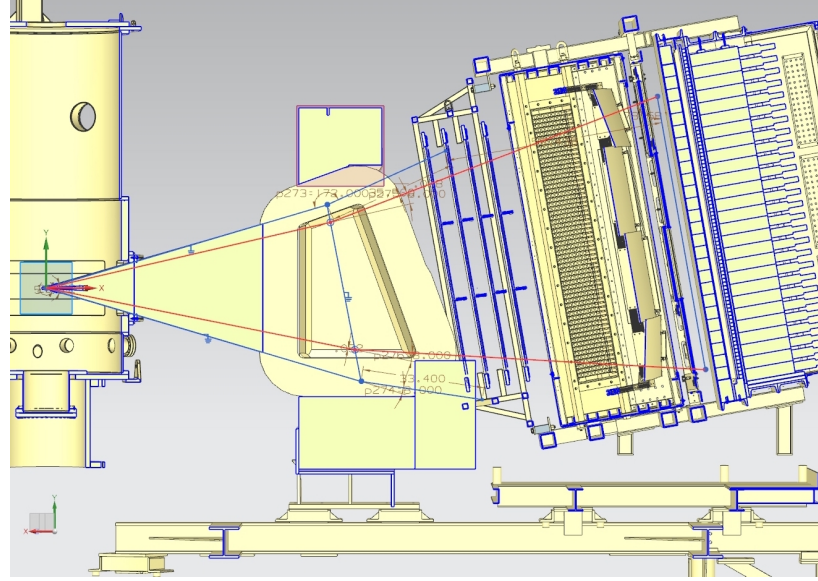


FIG. 4. The BigBite spectrometer with the upgraded detector stack.

202

1. Simulation of BigBite

203

2. Detector Package

- 204 a. Background Rate in BigBite
- 205 b. Front GEM chambers
- 206 c. Gas Cherenkov Counter
- 207 d. Rear GEM chamber
- 208 e. Shower and Preshower
- 209 f. Timing Scintillator Hodoscope

210

3. Trigger

211

4. Simulation of BigBite

212

a. Rates in the detectors

213

b. Trigger rate and efficiency

214

B. Neutron Detector

215 S

216

1. Structure of the Neutron Detector

217 **V. SIMULATIONS, ESTIMATIONS OF COUNTING RATES AND**
 218 **ACCIDENTALS**

219 The estimations of counting rates accidentals have been performed using G4SBS, the
 220 GEANT4-based simulation package developed for the SBS experiment [?]. This package
 221 includes a wide range of event generators, which allows to evaluate the rates for both events
 222 of interest (signal) and background. The representation of the experiment apparatus in
 223 G4SBS is shown in the high ϵ configuration on Fig. 5.

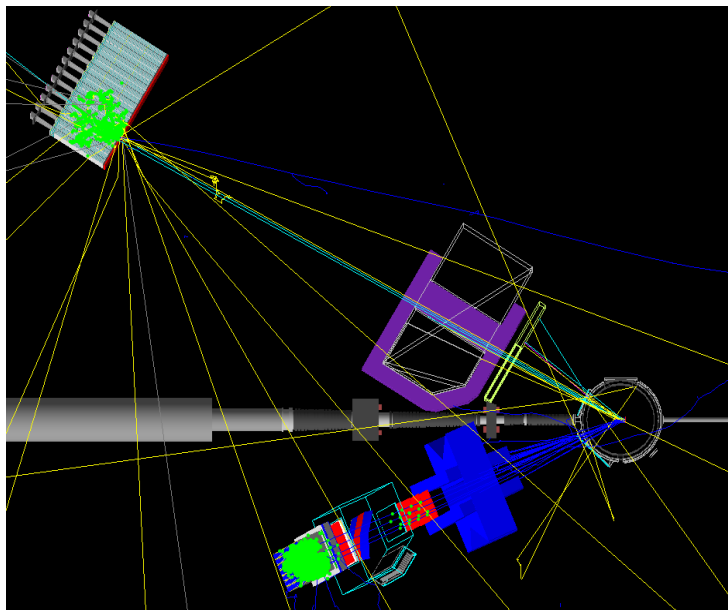


FIG. 5. Top view of the experimental apparatus model in G4SBS, shown in the high ϵ configuration. The beam direction is indicated, as well as the main elements (HCAL, SBS magnet, BigBite spectrometer)

224
 225

226 **A. Quasi-elastic counting rates**

227 The signals for this experiment have been generated using the G4SBS elastic/quasi-elastic
 228 generator. We generated 1M events sample for each kinematics, on a solid angle that was

²²⁹ larger than the detector acceptance. To evaluate the detector solid angle, we define simple
²³⁰ criteria that each event has to pass, defined as the following;

- ²³¹ • require a primary track, going through all 5 GEM layers (electron arm);
- ²³² • require non-zero energy deposit in both the preshower and shower (electron arm);
- ²³³ • require non-zero energy deposit in HCal (hadron arm).

²³⁴ The detector solid angle, for both proton and neutron, are defined in Table. I

Point (ϵ)	$\Delta\Omega_e$ (msr)	$\Delta\Omega_e \otimes \Delta\Omega_n$ (msr)	$\Delta\Omega_e \otimes \Delta\Omega_p$ (msr)
1 (0.599)	52.4	46.7	47.2
2 (0.838)	32.7	23.4	23.0

TABLE I. Kinematics solid angles and efficiencies.

²³⁵

²³⁶ Then, we evaluate the detection efficiency. For the electron, we require the energy recon-
²³⁷ structed in the BigBite calorimeter to be above a threshold defined as $thr = \mu_E - 2.5 * \sigma_E$,
²³⁸ as well as a minimum number of GRINCH PMTs fired due to the primary electron; For
²³⁹ HCal, we require the threshold to be such as we obtain 90% efficiency. These values are
²⁴⁰ summarized in Table. II.

Point (ϵ)	BB thr. (GeV)	HCal thr. (GeV)	η_e	η_n	η_p
1 (0.599)	1.32	1.06	0.902	0.904	0.892
2 (0.838)	2.99	0.09	0.807	0.887	0.876

TABLE II. Kinematics solid angles and efficiencies.

²⁴¹

²⁴² The counting rates are evaluated using the events that have passed the selection described
²⁴³ above, and weighting those events with the cross section calculated by G4SBS, multiplied
²⁴⁴ by the generation solid angle, using the formula:

$$N_{est} = \mathcal{L}\Delta t \times \sum_{i \in acc\ evts} \frac{d\sigma}{d\Omega} * \Delta\Omega_{Gen}/N_{Gen} \quad (8)$$

²⁴⁵ The counting rates for both kinematics are available in Table. III, assuming 12 hours of
²⁴⁶ running at an intensity of $30 \mu\text{A}$ on a 15cm liquid deuterium target, with density 0.169
²⁴⁷ g.cm^{-3} .

Point (ϵ)	QE $e-n$ counts	QE $e-p$ counts	F_n^2 ($\times 10^{-3}$)	ΔF_n^2 ($\times 10^{-6}$)	F_p^2 ($\times 10^{-3}$)	ΔF_p^2 ($\times 10^{-6}$)
1 (0.599)	1.68×10^6	4.57×10^6	1.09	0.84	2.97	1.39
2 (0.838)	4.52×10^6	1.21×10^7	0.92	0.43	2.53	0.79

TABLE III. Quasi-elastic counting rates, and “reduced cross section” as defined by Eq. ???. These rates assume 12 hours of running at an intensity of $30 \mu\text{A}$ on a 15cm liquid deuterium target, with density 0.169 g.cm^{-3} .

²⁴⁸

²⁴⁹ The calculation of the F_2 term requires the evaluation of the Mott cross section. The
²⁵⁰ Mott cross section has been calculated with the weighted average of the electron variables
²⁵¹ (momentum and polar angle).

Point (ϵ)	$\langle \theta_e \rangle$ (deg)	$\langle k' \rangle$ (GeV)	$\langle Q^2 \rangle$ (GeV 2)	σ_{Mott} (nb sr $^{-1}$)
1 (0.599)	41.7	2.01	4.47	6.62
2 (0.838)	22.9	4.26	4.40	48.0

TABLE IV. Cross-section weighted average of kinematic variables over the BigBite acceptance.
The Mott cross section has been evaluated at these values.

²⁵²

253

B. Background and trigger rates

254 The main processes expected to contribute the trigger rates for the BigBite spectrometer
 255 are:

- 256 • the inelastic electron nucleon scattering process;
 257 • photons from inclusive π^0 production;
 258 • and to a lesser extent, charged pions.

259 One the other hand, we expect all sorts of hadronic backgrounds to contribute to the rates in
 260 HCal, the dominant ones being pions. Both the inelastic scattering and the inclusive neutral
 261 and charged pion production are implemented in G4SBS, the latter relying on the Wiser
 262 parametrization [?]. We may also considered the minimum-bias “beam-on-target” gener-
 263 ator for the HCal background, especially at lower angle (all electromagnetic and hadronic
 264 processes being built-in in G4SBS).

265 The thresholds to apply to each arm are determined as a function of the elastic peak. For
 266 the electron arm, the threshold has been set at $\mu_E - 2.5\sigma_E$, μ_E and σ_E being respectively
 267 the position and width of the fitted elastic peak. Fig. 6 presents the distributions of rate of
 268 energy deposit for the different processes involved in the BigBite trigger rates.

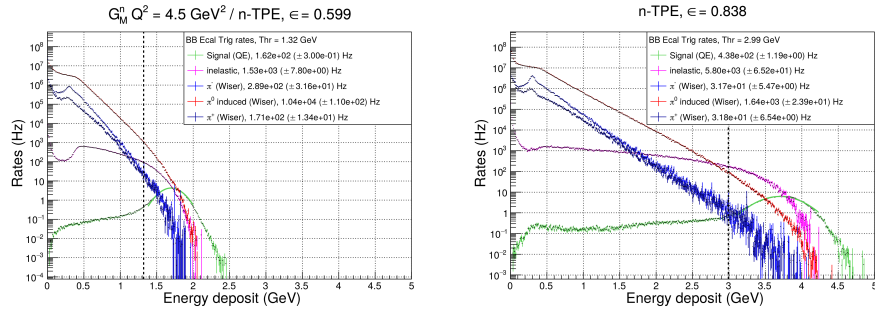


FIG. 6. Rates of the different process contributing to the BigBite electron arm trigger, for the low ϵ (left) and the high ϵ (right). Quasi-elastic is in green, inelastic in magenta, π^0 in red, π^- in blue, and π^+ in dark blue. Note the resolution for the elastic peak in the BigBite shower is ~ 0.3 GeV.

269

270

271 Since HCal is a sampling calorimeter (meaning that only a fraction of the shower energy
 272 is measured), it's resolution is significantly wider (~ 0.7 GeV). Due to this, the threshold
 273 is at 90% efficiency (which corresponds to ~ 0.1 GeV for both kinematics. Fig. ?? presents
 274 the distributions of rate of energy deposit for the different processes involved in the BigBite
 275 trigger rates.

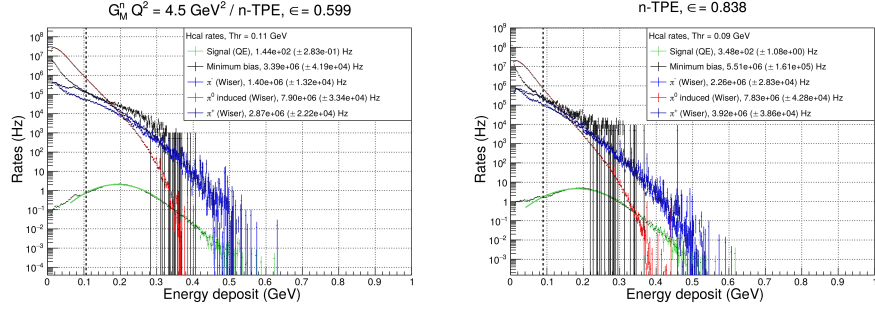


FIG. 7. Rates of the different process contributing to the HCal trigger, for the low ϵ (left) and the high ϵ (right). Quasi-elastic is in green, minimum bias in black, π^0 in red, π^- in blue, and π^+ in dark blue. Note the peak itself is around 0.2 GeV for 3.2 GeV nucleons.

276
 277
 278 The thresholds and trigger rates for each arm, as well as the coincidence rate (assuming
 279 30ns coincidence window), are summarized in Table. ??.

280
 281 Note that for HCal, the “total rates” is either the sum of inclusive charged and neutral pions
 282 evaluated with the Wiser cross sections *or* the “minimum bias” beam on target. We have
 283 good reasons to think that the Wiser code results actually overestimate the HCal rates, but
 284 for the sake of thoroughness, we have checked the coincidence rates assuming the sum of the
 285 inclusive pions (evaluated with the Wiser cross sections) as the HCal rates.

286 In the worst case scenario, the coincidence rates could be as high as 5kHz, which might be
 287 at the limit of manageability for the DAQ. However, a slight increase on the HCal threshold
 288 (which would drop the efficiency from $\sim 90\%$ to $\sim 85\%$) would decrease the total HCal rates by
 289 $\sim 35\%$ to 40% in this worst case scenario, which would make the situation more manageable
 290 (3.3 kHz).

Point (ϵ)	1 (0.599)		2 (0.838)	
	BigBite rates (Hz)	HCal rates (Hz)	BigBite rates (Hz)	HCal rates (Hz)
threshold (GeV)	1.32	0.106	2.99	0.090
Quasi-elastic	1.62×10^2	1.44×10^2	4.38×10^2	3.48×10^2
Inelastic	1.62×10^3	-	5.80×10^3	-
π^0 (Wiser)	3.16×10^2	1.40×10^6	3.17×10^2	2.26×10^6
π^+ (Wiser)	1.16×10^4	7.90×10^6	1.64×10^3	7.83×10^6
π^- (Wiser)	1.84×10^2	2.87×10^6	3.18×10^2	3.92×10^6
Minimum bias	-	3.39×10^6	-	5.40×10^6 (*)
<i>Total</i>	1.39×10^4	1.22×10^7	8.51×10^3	1.40×10^7
(min. bias - HCal only)		/ 3.39×10^6		/ 5.40×10^6
Coincidence rate	5.09×10^3		3.57×10^3	
(with min. bias HCal)	1.41×10^3		1.38×10^3	

TABLE V. Trigger rates for BigBite and HCal, with the different process contributions separated, and the sum. For HCal, the total rates is either the sum of the (Wiser) inclusive pions or the minimum bias. The coincidence rates assume a 30 ns coincidence window.

291

VI. PROPOSED MEASUREMENTS

292 We propose to use the same experimental setup of E12-09-019 experiment. We will add
 293 a kinematic point at $Q^2 = 4.5 \text{ (GeV/c)}^2$, but with a higher ϵ value. This additional point
 294 along with the data point of E12-09-019 experiment will allow us to perform LT separation
 295 and obtain (in one-photon approximation) the G_E^n value. Table 1 displays the kinematic
 296 setting of the proposed experiment.

Point	Q^2 (GeV/c) ²	E (GeV)	E' (GeV)	θ_{BB} degrees	θ_{SBS} degrees	ϵ (%)	$\Delta\sigma$ (%)	ΔTPE (%)
1	4.5	4.4	2.0	41.88	24.67	0.599		
2	4.5	6.6	4.2	23.23	31.2	0.838		

TABLE VI. Kinematic settings of the proposed experiment. The blue row is a kinematic point of E12-09-019 experiment.

297

298

VII. BEAM TIME REQUEST

299 **We request 48 hours total time (32 hours of beam-on target)** to measure the
 300 two-photon effect (and G_E^n in one-photon approximation) at $Q^2 = 4.5$ (GeV/c)² through a
 301 measurement of the cross sections of the reaction D(e,e'N) at a large value of the virtual
 302 photon polarization $\epsilon=0.84$. This experiment will take place in Hall A, utilizing the Big-
 303 Bite spectrometer to detect electrons scattered off the liquid deuterium target, and HCal
 304 calorimeter to detect the recoiling neutron and proton.

305 Data taking (if approved by PAC48) will take place in summer 2021 during the approved
 306 and scheduled run of the GMn, E12-09-019, experiment, which is going to measure the $e - n$
 307 elastic scattering cross section at $Q^2 = 4.5$ (GeV/c)² at $\epsilon=0.60$.

308 The set of instrumentation and required beam current for proposed measurement is iden-
 309 tical to one in the GMn experiment. The beam energy of 6.6 GeV will be used. One of two
 310 data points required for the cross section LT separation is already in the data taking plan of
 311 GMn.

312 There are no other measurements of TPE in the $e - n$ elastic scattering and knowledge
 313 of the TPE is essential for the understanding of the elastic electron scattering from neutron
 314 (and proton) and hadron structure. Furthermore, it is a necessary input in the analysis and
 315 interpretation of a wide range of electron scattering processes.

316 The kinematics of our measurements emphasize the same Q^2 range where TPE in $e - p$
 317 elastic scattering was observed to dominate in Rosenbluth slope. Measuring at this high
 318 momentum transfers will provide unique input for testing TPE calculations [4].

319 We propose to measure the Rosenbluth slope and extract (in one-photon approximation)
 320 $\delta G_E^n / G_M^n$ to an accuracy of 0.15, which would bring its precision to a level comparable with
 321 that of the double polarization experiments GEN-RP and GEN-He3 at such value of Q^2 .
 322 Such precision should be sufficient to detect the TPE contribution to the $e - n$ Rosenbluth
 323 slope on the three sigma level.

-
- 324 [1] R. Hofstadter, *Rev. Mod. Phys.* **28**, 214 (1956).
- 325 [2] M. N. Rosenbluth, *Phys. Rev.* **79**, 615 (1950).
- 326 [3] E. Christy *et al.*, “Two-photon exchange in electron-proton elastic scattering at large four-momentum transfer,” (2020), in preparation for publication in PRL.
- 327
- 328 [4] P. G. Blunden, W. Melnitchouk, and J. A. Tjon, *Phys. Rev.* **C72**, 034612 (2005), arXiv:nucl-th/0506039 [nucl-th].
- 329
- 330 [5] J. Arrington, P. G. Blunden, and W. Melnitchouk, *Prog. Part. Nucl. Phys.* **66**, 782 (2011), arXiv:1105.0951 [nucl-th].
- 331
- 332 [6] A. Afanasev, P. Blunden, D. Hasell, and B. Raue, *Prog. Part. Nucl. Phys.* **95**, 245 (2017), arXiv:1703.03874 [nucl-ex].
- 333
- 334 [7] B. Wojtsekhowski, in *Exclusive processes at high momentum transfer. Proceedings, Newport News, USA, May 15-18, 2002* (2002) arXiv:1706.02747 [physics.ins-det].
- 335
- 336 [8] G. D. Cates, C. W. de Jager, S. Riordan, and B. Wojtsekhowski, *Phys. Rev. Lett.* **106**, 252003 (2011), arXiv:1103.1808 [nucl-ex].
- 337
- 338 [9] G. A. Miller, *Phys. Rev. Lett.* **99**, 112001 (2007), arXiv:0705.2409 [nucl-th].
- 339 [10] C. E. Carlson and M. Vanderhaeghen, *Phys. Rev. Lett.* **100**, 032004 (2008), arXiv:0710.0835 [hep-ph].
- 340
- 341 [11] E. B. Hughes, T. A. Griffy, M. R. Yearian, and R. Hofstadter, *Phys. Rev.* **139**, B458 (1965).
- 342 [12] R. G. Arnold *et al.*, *Phys. Rev. Lett.* **61**, 806 (1988).
- 343 [13] L. Durand, *Phys. Rev.* **115**, 1020 (1959).
- 344 [14] E. E. W. Bruins *et al.*, *Phys. Rev. Lett.* **75**, 21 (1995).
- 345 [15] G. Kubon *et al.*, *Phys. Lett.* **B524**, 26 (2002), arXiv:nucl-ex/0107016 [nucl-ex].
- 346 [16] J. Lachniet *et al.* (CLAS), *Phys. Rev. Lett.* **102**, 192001 (2009), arXiv:0811.1716 [nucl-ex].
- 347 [17] V. Punjabi, C. F. Perdrisat, M. K. Jones, E. J. Brash, and C. E. Carlson, *Eur. Phys. J.* **A51**, 79 (2015), arXiv:1503.01452 [nucl-ex].
- 348